ASEG-PESA 2015
Geophysics and Geology together for Discovery
24th International Geophysical Conference and Exhibition
15–18 February 2015 Perth, Western Australia

Parametric 3D inversion of airborne time domain electromagnetics

Michael S. McMillan* Schwarzbach
University of British Columbia
2020-2207 Main Mall
Vancouver, B.C. Canada
mmcmilla@eos.ubc.ca

Douglas W. Oldenburg
University of British Columbia
2020-2207 Main Mall
Vancouver, B.C. Canada
doug@eos.ubc.ca

Eldad Haber
University of British Columbia
2020-2207 Main Mall
Vancouver, B.C. Canada
haber@math.ubc.ca

Christoph
University of British Columbia
2020-2207 Main Mall
Vancouver, B.C. Canada
cschwarz@eos.ubc.ca

SUMMARY

Conventional voxel-based inversion algorithms can encounter difficulties when inverting airborne time-domain electromagnetic data in three dimensions. In certain environments with these codes, it can be challenging to delineate sharp boundaries between geologic units with large conductivity contrasts and to accurately image thin conductive targets. Furthermore, spurious circular inversion artifacts, known as ringing, can occur around conductive targets.

To address these issues we have developed a parametric inversion code that can be used to find the optimal location, shape and conductivity value of a single anomaly in a homogeneous or heterogeneous background. The algorithm incorporates a Gauss-Newton optimization scheme in conjunction with a level set formulation to outline the anomaly of interest, and can be combined with a conventional voxel-based algorithm in more complicated geologic settings.

The code is shown to be successful with a synthetic data set over a thin dipping plate, and two field data sets. For the synthetic scenario, the parametric inversion recovers the true dip and size of a conductive target with no a priori information. The algorithm also accurately defines the extent of a diamondiferous kimberlite pipe and a dipping massive sulphide deposit beneath a conductive overburden.

Key words: parametric, inversion, electromagnetics, level sets,

INTRODUCTION

Airborne electromagnetic (AEM) surveys are an important part of many mineral exploration programs, especially when attempting to image buried conductors. When performing three-dimensional (3D) inversions on AEM data sets, conventional voxel-based inversions such as Oldenburg *et al.* (2013) can have difficulty in resolving thin targets or sharp boundaries between two contrasting resistivity units. With a typical least-squares regularization, this results in a smeared anomaly or border, which can pose problems during interpretation or drill targeting. Another issue is the circular nature of the sensitivity from a coincident loop airborne system, which can cause inversion artifacts known as ringing. This can result in conductive features to be erroneously placed around the true conductive target in a ring-like manner.

Parametric inversions are well researched methods of reducing the parameter space of an inverse problem (Dorn *et al.*, 2000; Zhdanov and Cox, 2013), and can alleviate some of the issues conventional inversions face. Parametric inversions can also be coupled with such methods as level sets (Osher and Sethian, 1988), and together they can solve for the boundary of a conductivity anomaly (Dorn *et al.*, 2000; Aghasi *et al.*, 2011). This enables a computationally efficient method of imaging compact anomalies and sharp boundaries with greater ease without the issue of ringing. Consequently, we incorporate a parametric inversion with level sets for time domain airborne electromagnetics, and demonstrate its applicability to both synthetic and field data sets.

METHODS

Our parametric approach searches for one anomaly of interest, either conductive or resistive, in a background of arbitrary conductivity. This background can either be a uniform half-space or a heterogeneous conductivity from a priori information or another inversion algorithm. The conductivity of the anomalous body can be fixed by the user, or the optimal conductivity can be a parameter in the inversion. In the case of a uniform background, the best-fitting background conductivity can also be found. The inversion solves time-dependent quasi-static Maxwell's equations

$$\nabla \times \mathbf{E} + \mu \mathbf{H}_t = 0 \tag{1}$$

$$\nabla \times \mathbf{H} - \sigma \mathbf{E} = \mathbf{s} \tag{2}$$

with a finite volume discretization where **E** and **H** are the electric and magnetic fields, subscript t is the time derivative, μ is the magnetic permeability, σ is the electrical conductivity and **s** is a source term. The anomalous conductivity body has the shape of a skewed Gaussian ellipsoid, which is defined by first calculating a smoothly varying function τ

$$\tau = c - (\mathbf{x} - \mathbf{x_0})^{\mathrm{T}} \mathbf{M} (\mathbf{x} - \mathbf{x_0}) \tag{3}$$

where *c* represents a positive constant, **x** is a vector of observation points in three dimensions, $\mathbf{x_0}$ is vector with spatial coordinates of the anomaly centre, and **M** is a 3 x 3 symmetric, positive definite matrix with skewing and rotation parameters. The function τ is passed to an analytic step-off function s

$$\mathbf{s}(\boldsymbol{\tau}) = \sigma_0 + 0.5\,(1 + \tanh(a\boldsymbol{\tau}))\,(\sigma_1 - \sigma_0) \qquad (4)$$

that assigns the conductivity to either a background (σ_0) or anomalous (σ_1) level. When τ = 0, also known as the zero level set, a transition zone occurs between σ_0 and σ_1 with a width controlled by the parameter *a*. The optimization of the inversion follows a Gauss-Newton procedure, where the sensitivity is composed of derivatives of the function **s** with respect to the inversion parameters. This optimization scheme is like many conventional voxel-based codes (Oldenburg *et al.*, 2013), but the regularization has been removed because our initial tests have empirically found it is not required. The inversion parameters however, are scaled to ensure a well-conditioned Gauss-Newton matrix, and a line search determines an appropriate step length. The program terminates once it has either reached a desired level of convergence, a maximum number of iterations, or when a suitable Gauss-Newton step can no longer be found. If desired, the parametric result can be set as the initial model for a conventional inversion to resolve additional features of interest. This process can be iterated to optimize both the anomalous body and surrounding background features.

RESULTS

Three examples will be discussed that showcase the versatility of this parametric code. The first is a synthetic model of a thin conductive dipping plate of 3 ohm-m in a background of 3000 ohm-m as shown in Figure 1a. The synthetic data are generated by simulating a coincident loop airborne EM survey with seven east-west lines with a line spacing and data spacing of 100 m. There are a total of 49 transmitter locations, each 37.5 m above topography. The data consists of 19 time channels between 10 µs and 7000 µs. Five percent Gaussian noise is added to the data prior to inversion. The initial starting guess consists of a 50 m radius sphere of 3 ohm-m centred over the anomaly at an elevation of 200 m below surface. The guess is designed to provide little in the way of a priori depth information and no dip information. The conductivity of the plate and background are kept fixed throughout the inversion.

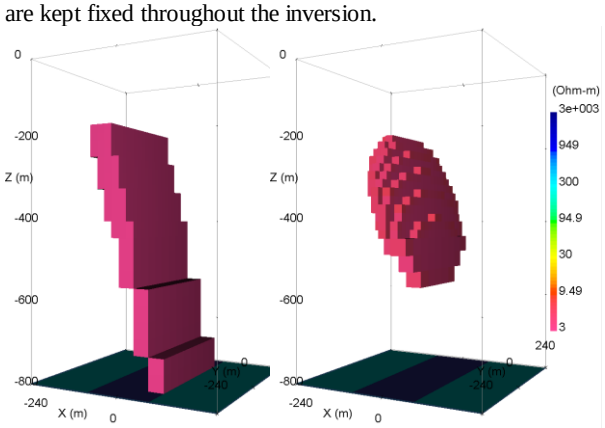

a) b)

Figure 1: a) Synthetic true model. Plate parameters: 3 ohm-m, 60m thick, 320m in strike length, depth extent ranges from 200m to 800m below surface. Background = 3000 ohm-m b) Parametric recovery.

After 31 Gauss-Newton iterations the parametric inversion result is shown in Figure 1b. The parametric recovery does a good job in depicting the true dip, width, and strike length of the dipping plate. The result is not able to image the conductor to depths lower than 600 m, and this could be a result of limited sensitivity to such depths. Figure 2 shows the good agreement between the observed and predicted data at a time channel of 1110 µs. In comparison, the result from a conventional inversion (Oldenburg *et al.*, 2013), albeit with a 3000 ohm-m half-space initial guess, is shown in Figure 3. The inversion in Figure 3 depicts the aforementioned ringing issue, consisting of conductive material placed around the target. This issue is avoided with the parametric code.

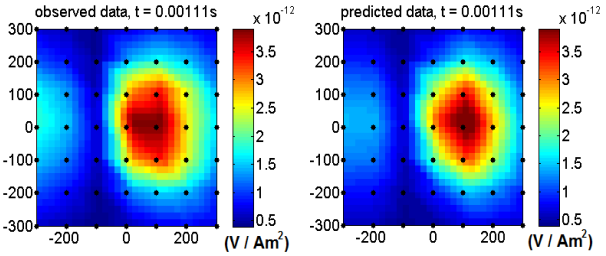

a) b)

Figure 2: a) Observed data at 1.11e-3 seconds b) Predicted data at 1.11e-3 seconds. The predicted data closely matches the observed data. Transmitter points shown as black dots.

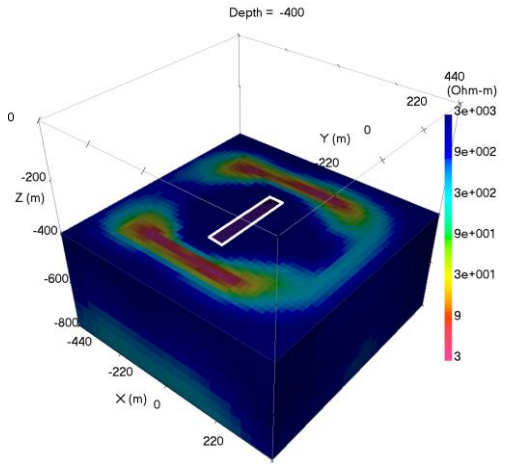

Figure 3: Synthetic inversion result at a depth of 400m using a conventional voxel-based inversion. The true outline of the dipping plate is shown in solid white. Ring-like structures occur around the true anomaly.

The second example comes from the Tli Kwi Cho (TKC), DO-27, diamondiferous kimberlite in the North-West Territories, Canada. A cross section through the kimberlite pipe, located in the Slave craton, is shown in Figure 4. This displays a mostly vertical pipe that widens as it approaches the surface (Harder *et al.*, 2008). In this setting, the conductivity of the background rock, which is primarily granite, is quite resistive, whereas the pyroclastic kimberlite itself possesses a more conductive signature, due to extreme alteration and the presence of serpentine (Eggleston *et al.*, 2014). This results in a noticeable

and distinct AEM anomaly, which is ideal for our parametric inversion.

In 2004, a Versatile Time Domain Electromagnetic (VTEM) survey measured z-component dB/dt data over the TKC kimberlite. Six east-west lines, with a line spacing of 75 m were inverted with the parametric code. The inversion includes a total of 194 transmitter locations, each with ten time channels between 90 µs and 350 µs. Later time channels exist but contain too much noise to be deemed beneficial.

The initial guess for the parametric inversion is a 150 m radius sphere of 1 ohm-m in a 1000 ohm-m background centred over the AEM anomaly. Unlike the synthetic example, the conductivity of the anomaly and background can freely change and Figure 5 portrays a cross-section through the resulting parametric model after 18 Gauss-Newton iterations, along the same Northing as the geologic image from Figure 4. The final conductivity values of the anomaly and background are 27 and 1009 ohm-m respectively. The resemblance between Figures 4 and 5 is quite similar, as the parametric inversion does an excellent job in capturing the boundaries of the kimberlite, and even the slight dip to the West. Observed and predicted data agree to a satisfactory level.

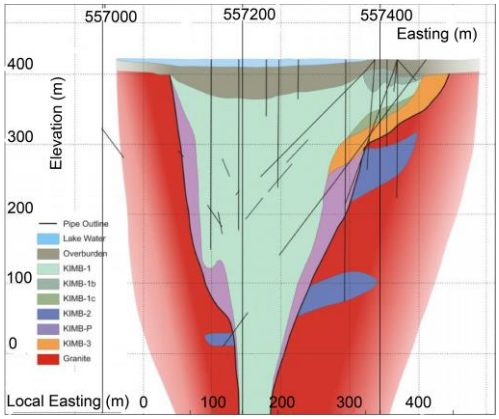

Figure 4: Geologic cross section through the DO-27 kimberlite at a Northing of 7133829. Image modified from Harder *et al.*, (2008).

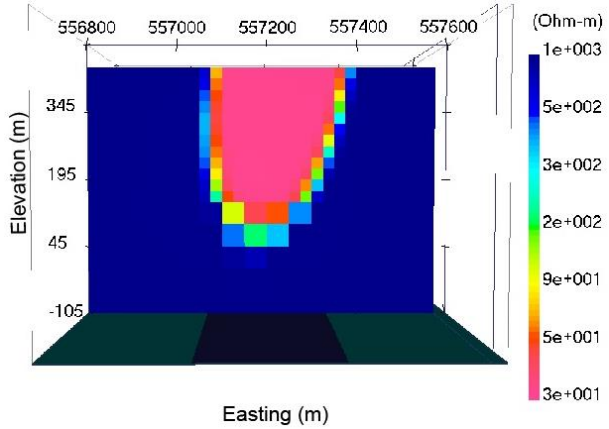

Figure 5: Parametric cross-section through the DO-27 kimberlite at a Northing of 7133829. There is a strong agreement with the geologic cross section in terms of the size and shape of the anomaly.

The final example is from the Caber volcanogenic massive sulphide (VMS) deposit in Quebec, Canada where the target is a thin dipping conductor. In 2012, eight lines of z-component dB/dt AEM data over the deposit were acquired with the VTEM-35 system. Lines were separated by 50m for a total of 102 transmitter locations. Time channels ranged from 505 µs to 2021 µs. A simplified cross-section through the deposit is displayed in Figure 6 (Legault *et al.*, 2010). This image illustrates a steep South-West dipping mineralized area next to a shear zone in amongst a host of resistive intrusive rocks underneath a conductive overburden. The mineralized region, coupled with the adjacent shear zone, represent the conductive target of interest. However, in this setting, the conductive overburden represents another conductive feature to consider.

We approach this issue by first inverting for the mineralized zone with the parametric code, and importing the result into a conventional voxel-based EM inversion code to fill in the background features such as the overburden layer. The process can be iterated multiple times if needed, but for this example we performed a parametric and conventional inversion only once, with 12 Gauss-Newton iterations needed for the parametric code. Due to the more complex geologic setting, we applied a more sophisticated starting model based on a priori information (Prikhodko *et al.*, 2012). This was a near-vertical 100m thick, 0.13 ohm-m thin plate in a 1000 ohm-m background. The final inversion conductivity values are 0.07 ohm-m and 2042 ohm-m respectively.

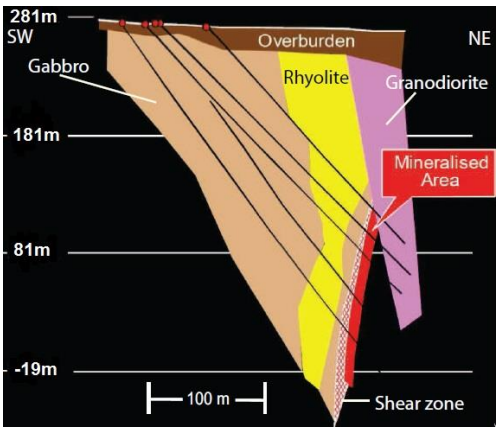

Figure 6: Geologic cross section through the Caber volcanogenic massive sulfide deposit. Image modified from Legault *et al.*, (2010).

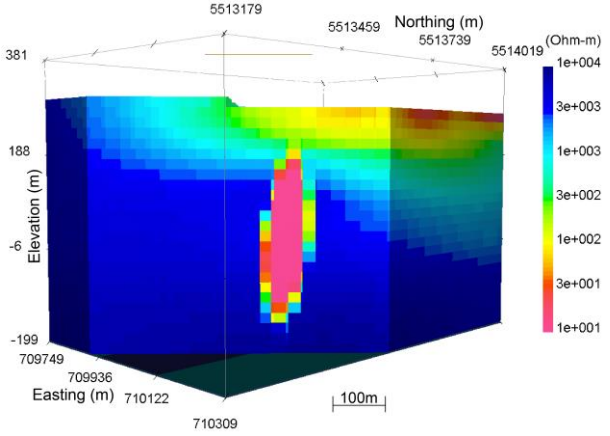

Figure 7: Cross section through the parametric recovery of the Caber deposit, with the smooth background incorporated. The dip of the anomaly and overburden agree nicely with Figure 6.

A cross section through the resulting model at the centre of the deposit is shown in Figure 7. This image demonstrates the ability to combine the parametric code to image both the target of interest as well as the near-surface overburden layer. The dip of the target matches the geologic cross-section nicely, and a thin overburden exists over the anomaly and thickens to the North-East as does the cross-section in Figure 6. Some differences do occur as the parametric recovery is slightly wider than what the geologic cross-section suggests and extends to a deeper depth.

CONCLUSIONS

We developed a parametric algorithm to invert time-domain airborne electromagnetic data and showed that it can be applied to synthetic and field data sets to resolve a number of different targets. The inversion recovers the location and skewing parameters of the anomaly of interest as well as the optimal conductivity value for the target and background if desired. The shape of the anomaly is based on a Gaussian ellipsoid, and the code requires initial guesses for the inversion parameters, after which it follows a Gauss-Newton optimization schedule until a suitable model is found. The result of this parameterization can then be input as the initial model for a conventional voxel-based inversion code to resolve further features of interest.

The parametric inversion proved to be successful in resolving a synthetic buried thin dipping plate, a kimberlite pipe and a buried dipping plate below a conductive overburden. For more complicated target geometries, the parametric code would need to be modified to allow for the recovery of multiple anomalies, and this is the topic of future research.

ACKNOWLEDGMENTS

The authors thank members of UBC-GIF for their help working on the TKC deposit, as well as Geotech Ltd. for supplying the VTEM-35 data and a priori information regarding the Caber deposit.

REFERENCES

Aghasi, A., Kilmer, M., Miller, E., 2011, Parametric level set methods for inverse problems: SIAM Journal of Imaging Sciences, 4, 2, 618-650.

Dorn, O., Miller, E., Rappaport, C., 2000, A shape reconstruction method for electromagnetic tomography using adjoint fields and level sets: Inverse Problems, 16, 1119–1156.

Eggleston, T., Brisebois, K., Pell, J., 2014, Peregrine Diamonds Ltd., Lac de Gras Project, NWT, Canada, 43-101 Technical Report.

Harder, M., Hetman, C., Smith, B., Pell, J., 2008, The evolution of geological models for the DO-27 kimberlite, NWT, Canada, implications for evaluation: 9th International Kimberlite Conference Extended Abstracts. 1-3.

Legault, J., Prikhodko, A., Morrison, E., Bagrianski, A., Kuzmin, P., Tishin, P., 2010, Evolution of VTEM technical solutions for effective exploration: ASEG Expanded Abstracts, 1–4.

Oldenburg, D., Haber, E., Shekhtman, R., 2013, Three dimensional inversion of multisource time domain electromagnetic data: Geophysics, 78, E47-E57.

Osher, S., and Sethian, J., 1988, Fronts propagation with curvature dependent speed: algorithms based on Hamilton–Jacobi formulations: Journal of Computational Physics, 56, 12–49.

Prikhodko, A., Eadie, T., Fiset, N., Mathew, L., 2012, VTEM-35 test results over the Caber and Caber North Deposits: Geotech Technical Report.

Zhdanov, M., Cox, L., 2013, Multinary inversion for tunnel detection: IEEE Geoscience and Remote Sensing Letters, 10, 5, 1100-1103.